Title

The ionophore thiomaltol induces rapid lysosomal accumulation of copper and apoptosis in melanoma.

Journal

Metallomics : integrated biometal science, 14(1)

ISSN

1756-5901

Authors

Scrivner, Ottis
Dao, Long
Newell-Rogers, M Karen
et al.

Publication Date

2022

DOI

10.1093/mtomcs/mfab074

Peer reviewed

Metallomics, 14, 2022, mfab074
https://doi.org/10.1093/mtomcs/mfab074
Advance access publication date: 27 December 2021
Paper

The ionophore thiomaltol induces rapid lysosomal accumulation of copper and apoptosis in melanoma

Ottis Scrivner[1], Long Dao[2], M. Karen Newell-Rogers[2], Babbak Shahandeh[3], Frank L. Meyskens[3], Susan Kurumi Kozawa[4], Feng Liu-Smith[4], Germán Plascencia-Villa[5], Miguel José-Yacamán[6], Shang Jia[7], Christopher J. Chang[7,8] and Patrick J. Farmer[1,*]

[1]Department of Chemistry & Biochemistry, Baylor University, Waco, TX 76706, USA, [2]Department of Medical Physiology, College of Medicine, Texas A&M Health Sciences Center, Bryan, TX 77807, USA, [3]Department of Medicine, UC Irvine, Irvine, CA 92617, USA, [4]Department of Preventive Medicine, University of Tennessee Health Science Center, Memphis, TN 38163, USA, [5]Department of Neuroscience, Developmental and Regenerative Biology, The University of Texas at San Antonio, San Antonio, TX 78249, USA, [6]Applied Physics and Materials Science Department and MIRA Center, Northern Arizona University, Flagstaff, AZ 86011, USA, [7]Department of Chemistry, University of California, Berkeley, CA 94720, USA and [8]Department of Molecular and Cell Biology, University of California, Berkeley, CA 94720, USA

*__Correspondence:__ Department of Chemistry & Biochemistry, Baylor University, Waco, TX 76706, USA. E-mail: Patrick_Farmer@baylor.edu

Abstract

In this report, we investigate the toxicity of the ionophore thiomaltol (Htma) and Cu salts to melanoma. Divalent metal complexes of thiomaltol display toxicity against A375 melanoma cell culture resulting in a distinct apoptotic response at submicromolar concentrations, with toxicity of $Cu(tma)_2$ > $Zn(tma)_2$ >> $Ni(tma)_2$. In metal-chelated media, Htma treatment shows little toxicity, but the combination with supplemental $CuCl_2$, termed Cu/Htma treatment, results in toxicity that increases with suprastoichiometric concentrations of $CuCl_2$ and correlates with the accumulation of intracellular copper. Electron microscopy and confocal laser scanning microscopy of Cu/Htma treated cells shows a rapid accumulation of copper within lysosomes over the course of hours, concurrent with the onset of apoptosis. A buildup of ubiquitinated proteins due to proteasome inhibition is seen on the same timescale and correlates with increases of copper without additional Htma.

Keywords: copper ionophore, thiomaltol, melanoma, apoptosis, proteasome inhibition

Graphical abstract

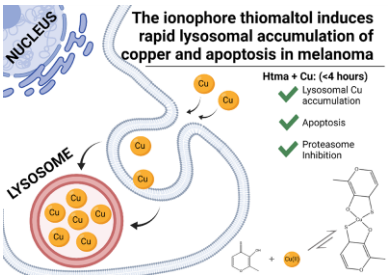

Treatment of A375 human melanoma with Htma and $CuSO_4$ results in lysosomal copper accumulation and apoptosis.

Introduction

Skin cancer is estimated to be the most common type of cancer in the USA; one in five Americans will develop skin cancer in their lifetime.[1] While melanoma makes up only 3% of this large population of skin cancers, it accounts for more than 75% of total skin cancer deaths.[2] Over the past decades, melanoma has increased to the fifth most common invasive cancer.[3] In 2002, the Davies group reported the discovery of a BRAF kinase mutation in 50–60% of advanced, invasive melanomas. Of these melanoma cases containing BRAF mutations, approximately 80% have a valine to glutamate amino acid substitution at the 600th position (BRAFV600E) arising from a single nucleotide polymorphism.[4] Subsequent research found that Cu(I) is required for BRAF-related signaling, specifically MEK1/2 requiring two Cu(I) atoms for kinase activity.[5,6] These studies have shown that melanoma cell growth is considerably decreased when cellular access to Cu(I) is limited.

Both melanoma cell cultures and melanoma in transgenic mice experiments can limit cellular Cu(I) by knockout of the gene responsible for coding CTR-1, the major high affinity Cu(I) transport protein. Limiting Cu(I) is problematic and difficult in human patients due to the necessity of Cu(I) as a cofactor in many enzymes including ceruloplasmin, Cu/Zn superoxide dismutase, cytochrome c oxidase, tyrosinase, and dopamine β-monooxygenase.[7] Paradoxically, recent research has shown that compounds that can act as ionophores increasing intracellular Cu have significant toxic effect on melanoma and other cancers.[8,9]

Received: September 27, 2021. **Accepted:** December 5, 2021

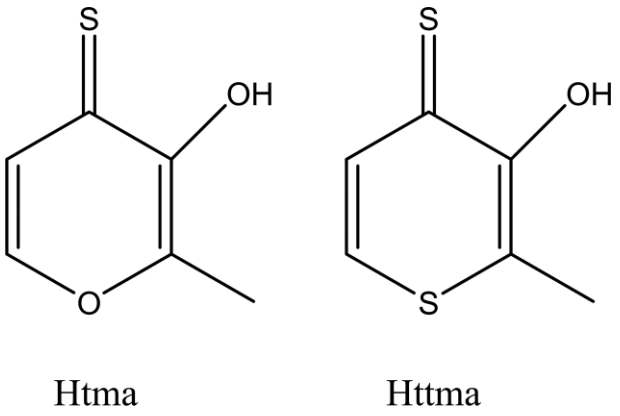

Scheme 1 Chemical structures of thiomaltol (left) and dithiomaltol (right).

Early reports of Cu-dependent toxicity to melanoma were reported for disulfiram (DSF), an FDA-approved treatment for alcohol abuse,[10] and Elesclolmol, a first-in-class FDA-approved drug for treatment of metastatic melanoma.[11] We reported that DSF's toxicity was dependent on available Cu; increasing levels of extracellular Cu results in significantly increased intracellular concentration and stronger apoptotic response in the melanoma.[12] In the following years, many Cu chelates with selective toxicity to cancers have been reported. Several were found to induce apoptosis, such as $Cu(pdtc)_2$,[13,14] $Cu(OHQ)_2$,[15] $Cu(PT)_2$,[16] $Cu(CQ)_2$[17]; Cu(Dp44mT) and other thiosemicarbazones complexes were suggested to induce apoptosis by disrupting lysosome integrity,[18] or disrupting the ER thiol redox status,[19] while one is suggested to inhibit ferroptosis.[20] Others complexes like $Cu(HK)_2$[9] and Cu-pyrazole-pyridine/Cu-pyrazole-pyrazole complexes induce paraptosis.[21] Even the previously discussed Cu-DSF complex, which has a strong literature-based precedent for apoptotic activity,[22–26] has been reported in some cases to exert a paraptosis,[21] and ferroptosis[27] in different cancer cell lines. Although apoptosis, paraptosis, and ferroptosis are all forms of programmed cell death, they differ in biochemical and morphological changes. Apoptosis, activated through either an intrinsic or extrinsic pathway, leads to a caspase cascade, cellular membrane blebbing, and DNA fragmentation.[28,29] Paraptosis involves cytoplasmic vacuolization, mitochondrial swelling, and absence of DNA fragmentation.[30,31] Ferroptosis is characterized by the accumulation of lipid peroxides,[32] triggering inflammation through the release of 'danger' molecules that activate the immune system and promote pathological inflammatory responses.[33]

Many Cu ionophores have also been shown to inhibit the ubiquitin-proteasome, which can lead to both paraptotic and apoptotic responses.[15,34] It is proposed that the ionophores help deliver Cu(II) to the 20S core particle of the 26S proteasome resulting in a loss of both trypsin and chymotrypsin proteolytic activity as well as a build-up of proteins marked for degradation by ubiquitination. This build-up of ubiquitinated protein triggers and eventually overwhelms the unfolded protein response (UPR) leading to intolerable endoplasmic reticulum (ER) stress and apoptotic cell death.[35,36] On the other hand, redox active Cu ionophores may generate oxidative stress characteristic of ferroptosis and induce lysosomal membrane permeabilization.[37,38] The current mechanisms underlying Cu ionophores induction of apoptosis, paraptosis, or ferroptosis dependent on the ionophore and cell type are not well understood, and more research in field is needed.

The Cu chelators thiomaltol (Htma)[39,40] and dithiomaltol (Httma)[41] shown in Scheme 1 have been previously studied in chemical[42,43] and biological studies.[44] Both ionophores induce a Cu-dependent apoptotic response in melanoma akin to that

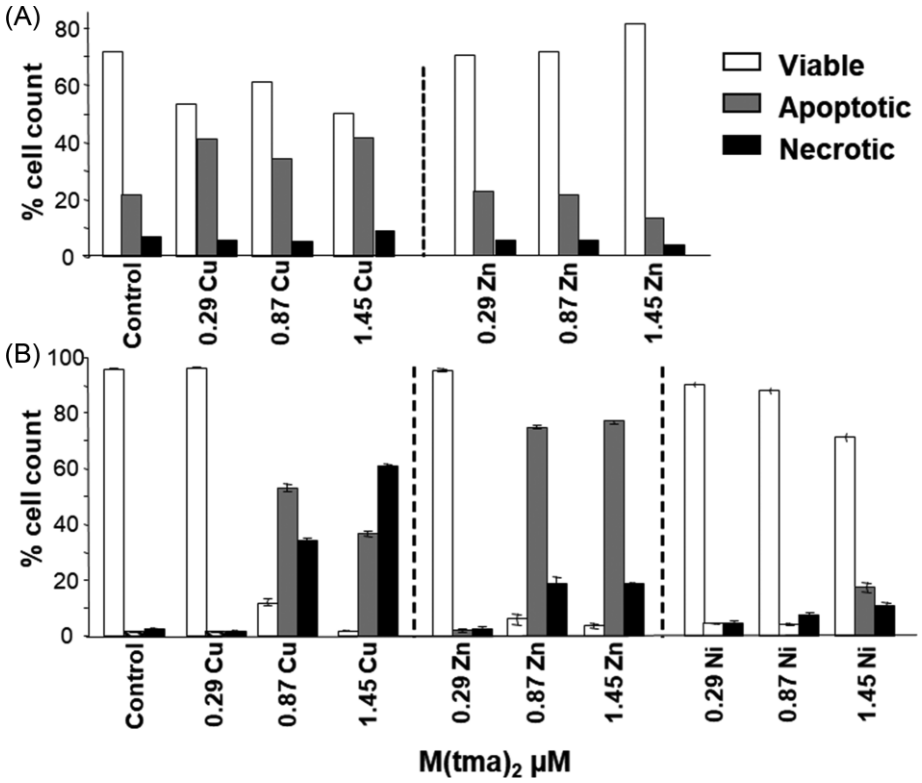

Fig. 1 Cytotoxicity measured by flow cytometry using Annexin V/PI after 24-h treatment in FBS-supplemented media with divalent $Zn(tma)_2$, $Cu(tma)_2$, and $Ni(tma)_2$ complexes towards (A) primary epidermal melanocytes and (B) A375 melanoma.

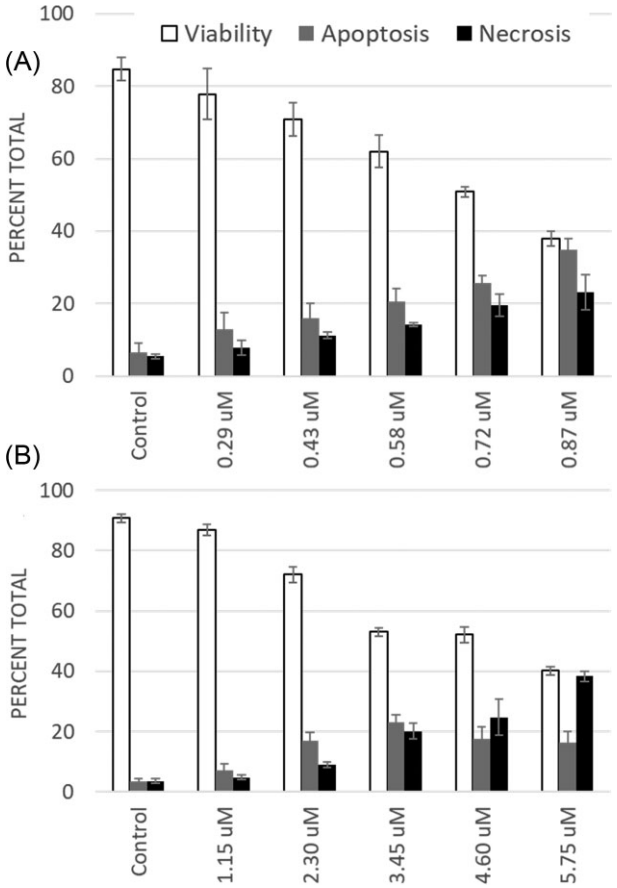

Fig. 2 Dose-dependent toxicity measured by flow cytometry after 24 h of treatment of A375 melanoma in chelexed media with (A) $Cu(tma)_2$ and (B) $Zn(tma)_2$.

Table 1. IC_{50} values from MTT assay of viability after 24 h

	IC_{50} (μM)		
Cell line	**$Cu(tma)_2$**	**$Ni(tma)_2$**	**$Zn(tma)_2$**
A375	0.30 ± 0.03	2.03 ± 0.25	5.07 ± 0.62
WM3211	0.37 ± 0.10	1.03 ± 0.14	5.18 ± 0.46
SK-Mel5	0.36 ± 0.01	2.22 ± 0.16	8.24 ± 0.19
SK-Mel28	0.24 ± 0.02	1.26 ± 0.18	5.29 ± 0.27
NHDF	0.39 ± 0.07	0.58 ± 0.12	4.25 ± 0.13

of DSF.[45,46] Htma has also been shown to be one of a handful of ionophores that showed metal-dependent anti-fungal treatment against *Cryptococcus neoformans*.[47] It was suggested that the lipophilicity of the active metalated ionophores allowed them to act as Cu transport chaperones in a manner similar to ionophores ATSM and GTSM.[48]

The actual modes of action of DSF, Htma, and other cancer-killing chelators are likely multifaceted, but data also suggest the Cu transport system itself is a common target. There is a long history of DSF and other dithiocarbamates inhibiting the embryonic development of fish and other small organisms.[49] For instance, exposure of embryonic zebrafish ova to DSF elicits pericardial edema, enlarged ventricles, and abnormal notochord development indicative of severe copper deficiency.[50] These same defects are seen in zebrafish embryos with lethal mutations to the Cu transporter Atp7A.[51,52] Analogous effects are seen in Htma

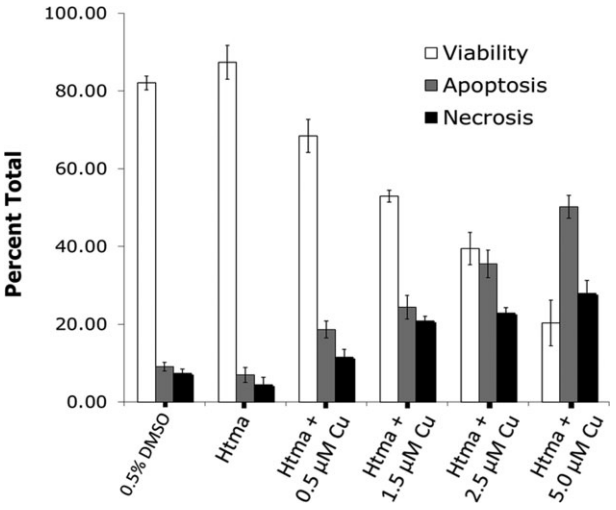

Fig. 3 Viability of melanoma cells treated with 0.7 μM Htma and increasing [$CuCl_2$] after 24 h, mean ± S.D., n = 3.

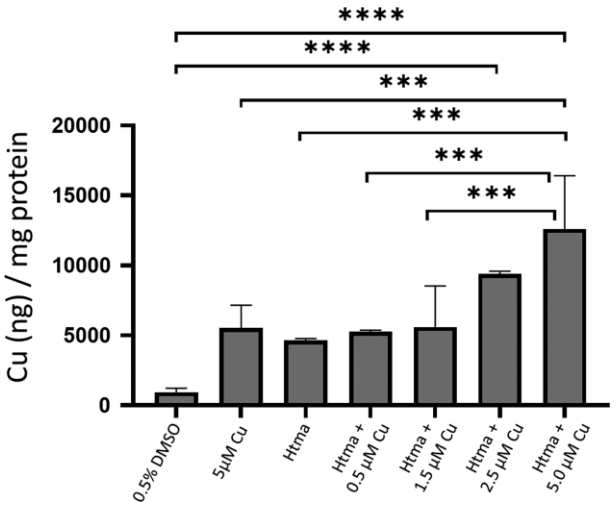

Fig. 4 Measurement of intracellular [Cu] in A375 melanoma cells by ICP-MS after treatment with 0.7 μM Htma and varying [$CuSO_4$] for 24 h. $P < 0.05$; mean ± S.D., n = 3.

treated zebrafish ova; co-treatment with copper salts is seen to exacerbate the effect for Htma but not for DSF.[53]

In this report, we examine time-dependent effects of Htma and metal ion combinations on A375 melanoma cells regarding the induction of apoptosis, accumulation of Cu, and inhibition of proteasome activity.

Results and discussion

$M(tma)_2$ toxicity against cell culture

Initial investigations found that several first row transition metal ion complexes of thiomaltol show higher toxicity towards A375 melanoma cells as compared to melanocytes. The flow cytometry data in Fig. 1 show submicromolar toxicity by both Cu and Zn complexes.

Because Htma may complex with a variety of divalent metal ions,[39] other metal ions in the growth media could inadvertently affect the toxicity. To avoid this, Chelex® 100 beads were used to remove any metal ions in the serum used before drugging. Figure 2 shows submicromolar LD_{50} for the $Cu(tma)_2$ in chelexed media,

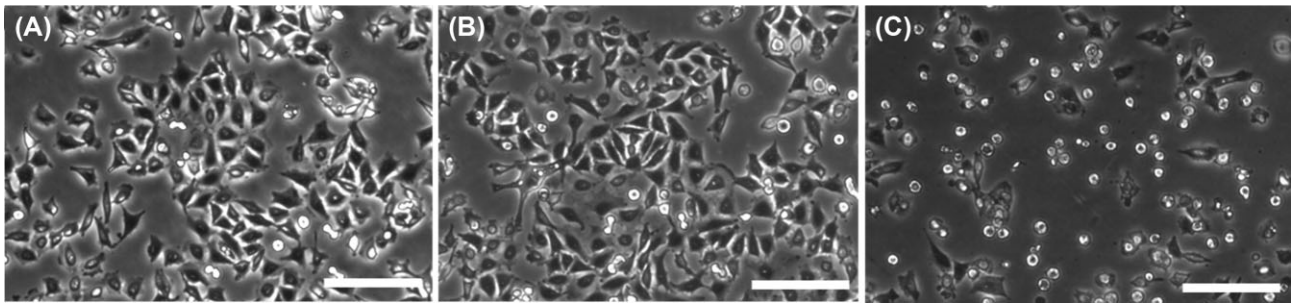

Fig. 5 Contrast images of A375 cells treated for 3 h with (A) 0.5% DMSO control, (B) 0.7 μM Htma, and (C) 0.7 μM Htma + 2.5 μM $CuSO_4$. Scale bars = 100 μm.

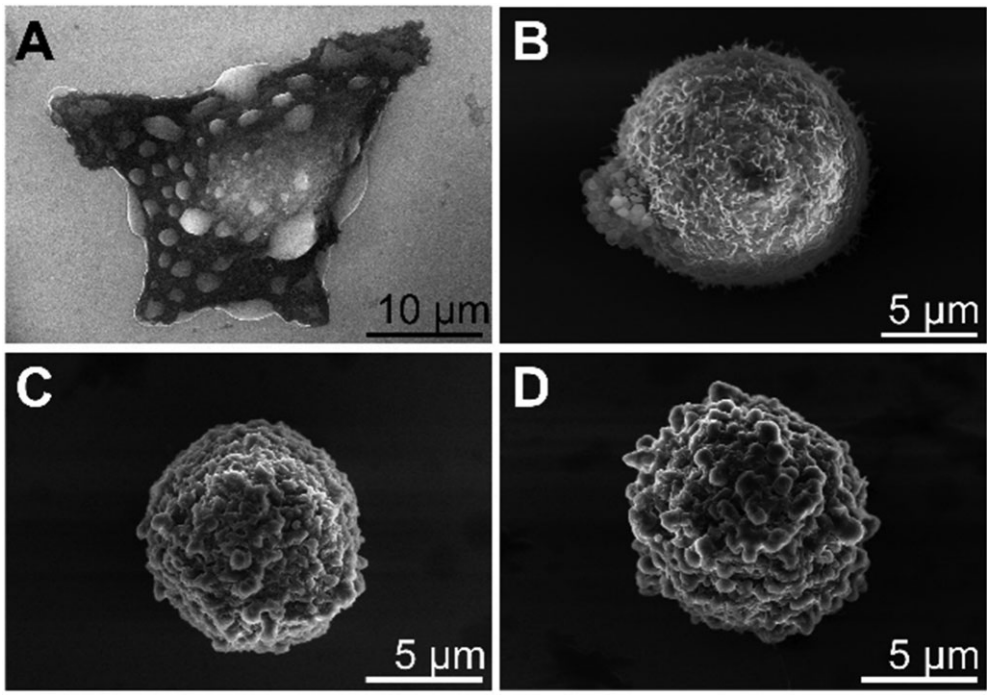

Fig. 6 Scanning electron microscopy of Cu/Htma-treated melanoma cells (2.5 uM $CuCl_2$ with 0.8 uM Htma). Images show scans of cells (A) prior to treatment, after (B) 1 h treatment, (C) 5 h of treatment, and (D) 6 h of treatment.

while the $Zn(tma)_2$ reaches a similar LD_{50} beyond 4 μM (further data are given in supplemental Fig. S1). These results suggest that Cu is largely responsible for the toxicity of Htma in melanoma.

A survey of the toxicity of these complexes towards other melanoma cell lines using the MTT and cell counting assays gave similar results (Table 1, supplemental Figs. S2–S4). The survey also revealed significant toxicity of the Cu and Ni complexes towards normal human dermal fibroblasts, NHDF, used as a noncancer control.

Htma toxicity dependent on accumulation of Cu within the cells

Like DSF, addition of excess copper amplifies Htma toxicity, as shown in Fig. 3. The melanoma cells remain viable with Htma treatment in chelated media but the addition of increasing concentrations of $CuCl_2$ resulted in an increased apoptotic and necrotic cell death. Importantly, note that 0.7 μM Htma would effectively complex with 0.35 μM Cu in a stoichiometric manner, yet a proportional increase in toxicity is seen as Cu concentrations exceed this stoichiometric ratio.

Inductively coupled plasma mass spectrometry (ICP-MS) measurements of the intracellular Cu concentrations of A375 cells drugged in unchelated media also show increases with increasing supplemental copper **(**Fig. 4). A T-test was performed at the 95% confidence interval, and the quantity of Cu in 0.7 μM Htma + 5 μM $CuSO_4$ is significantly different than individual 0.7 μM Htma or 5 μM $CuSO_4$ experiments. Based on these results, subsequent experiments utilized high Cu to Htma ratios, which we term as Cu/Htma treatments.

Cu/Htma treatment causes rapid morphological changes in melanoma cells

Although the dose–response experiments were conducted over 24 h, it was obvious that high Cu/Htma ratios induced cell death over a few hours, as illustrated in Fig. 5. This rapid cellular response was investigated by use of ultrahigh-resolution scanning and transition electron microscopy (SEM and TEM), previously

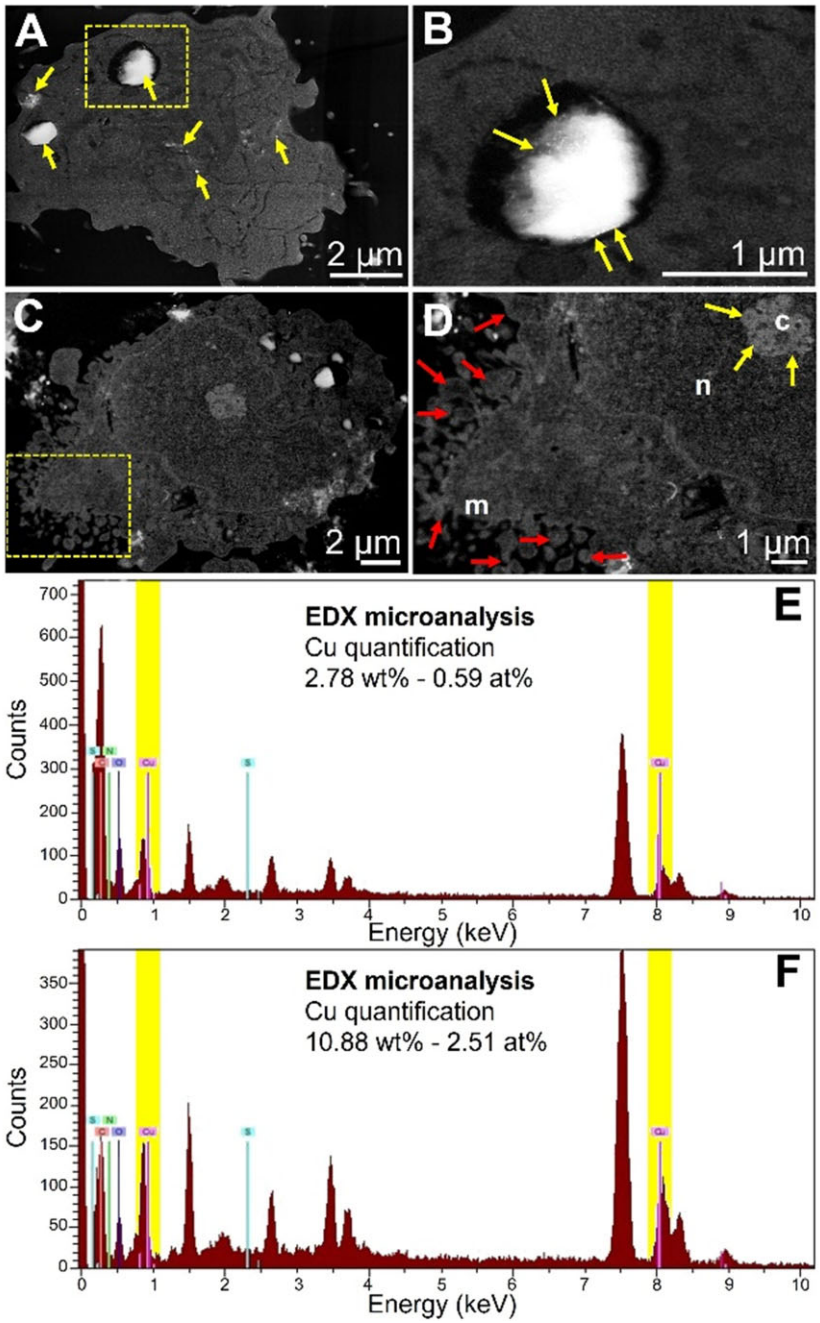

Fig. 7 Ultrastructural and EDX microanalysis of Cu/Htma treated cell after 1–5 h. (A) ADF-STEM of ultrathin section (arrows indicate electron-dense materials). (B) High magnification ADF-STEM of the selected area in (A), arrows indicate electron-dense materials within lysosomes. (C) ADF-STEM of ultrathin section Cu/Htma treated cell after 5 h. (D) High magnification ADF-STEM of selected area in (D), red arrows indicate blebbing in membrane (m) and yellow arrows indicate chromatin condensation (c) in nucleus (n). (E) EDX microanalysis of (A) indicating the percentage of copper (F) EDX microanalysis of the area in (D) indicating the percentage of copper.

used to characterize alternate modes of cell death.[54,55] SEM scans of whole A375 cells visualize morphological changes over a few hours following Cu/Htma treatment (Fig. 6). Panel A shows a cell at 0 h (before treatment) with the distinctive cell shape of melanoma cells. After 1 h of Cu/Htma treatment, the cells started to present alterations in cell membrane with the formation of blebbing (panel B) indicative of apoptotic responses. After 5 or 6 h of treatment, the morphological alterations are evident (panels C and D) with a significant number of protrusions, shrinking, rounded up, and detachment from the cell culture surface; all these signs are indicative of profound activation of apoptotic responses.[56,57] Furthermore, the melanoma cells showed retraction of pseudopods and significant reduction of cellular volume.

At the ultrastructural level, the cells showed reduction of nuclear volume, fragmentation, and chromatin condensation, as observed by Annular Dark-Field UHR-FE-STEM (Fig. 7). Furthermore, this technique revealed the accumulation of electron-dense materials (high-contrast white areas) in melanoma cells, particularly into vacuoles and small dense cores in the cytoplasm, as indicated with arrows in Fig. 7. Energy dispersive X-ray (EDX) microanalysis

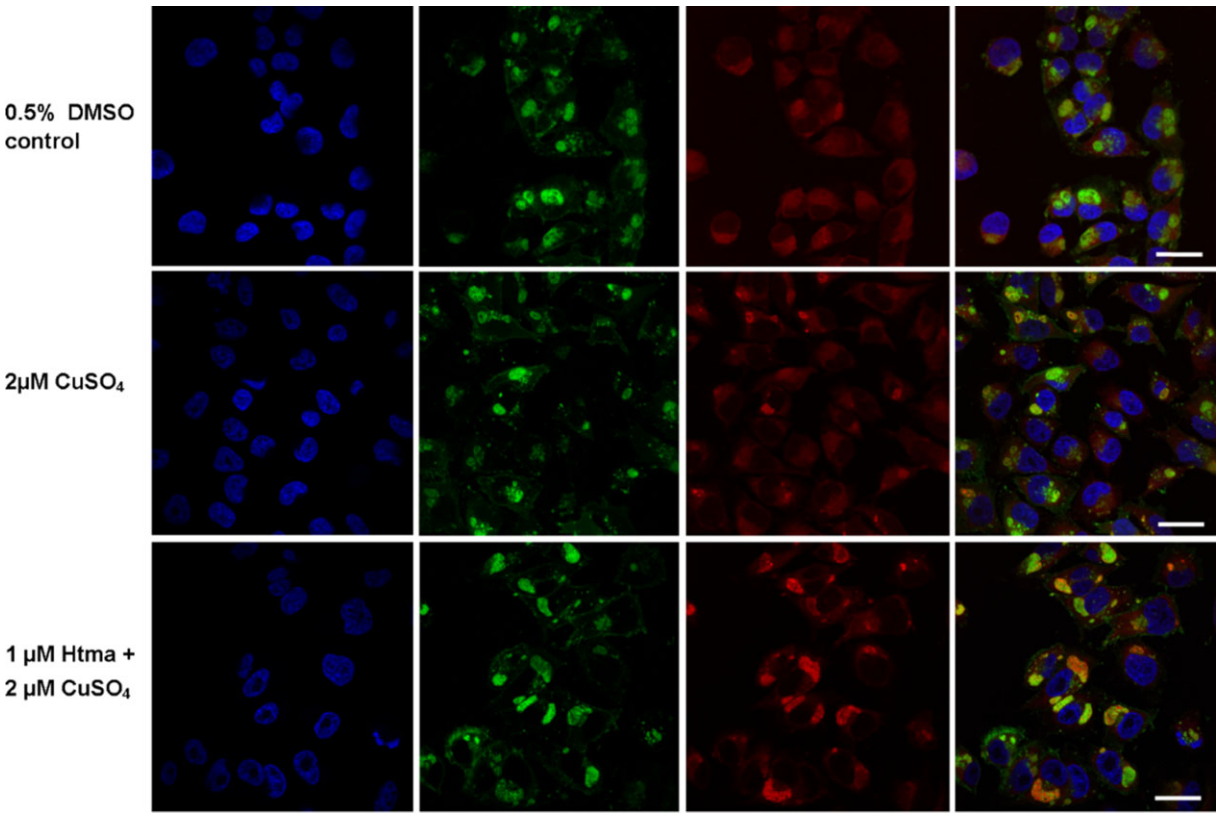

Fig. 8 Cu/Htma treatment selectively results in hyperaccumulation of Cu(I) in lysosomes. Cells were transduced with a GFP-tagged LAMP1 protein (green) using a CellLight® BacMam 2.0 reagent for 48 h, treated with Cu/Htma for 2 h, then loaded with CF4 Cu-probe (red) for 10 min, and then mounted with DAPI (blue). Images are representative of three independent experiments. Scale bars = 20 μm.

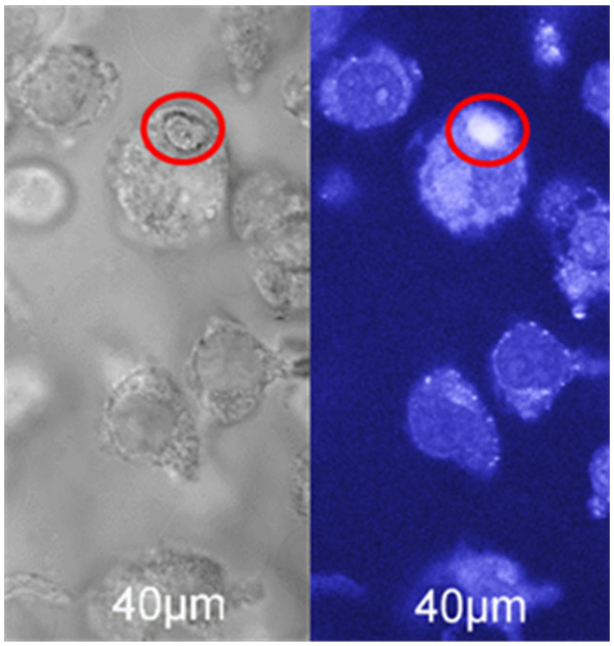

Fig. 9 Dark field (left) and fluorescent (right) images of A375 cells 1 h after treatment with 1 uM $Zn(ttma)_2$; red circle indicates high accumulation in a vacuole or lysosome.

of selected areas allowed to reveal the chemical signature of the samples.

We determined that the area corresponding to a complete cell had ca. 2.78 ± 0.34% weight of Cu (or 0.59 ± 0.05% atoms); this amount was determined by integration of the corresponding EDX peaks of Cu, centered at 0.930 and 8.040 keV (highlighted in Fig. 7B), in addition to the characteristic X-ray peaks of C, O, N, and S. Here, the X-ray peaks of Os (at 1.910 and 8.910 keV) and Ni (at 0.851 and 7.477 keV) corresponding to staining and TEM grids, respectively, were not included in the EDX microanalysis, to represent only the relative composition of the biosamples. High magnification Annular Dark-Field UHR-FE-STEM of the selected area indicated in Fig. 7A revealed morphological details of the melanoma cells; the electron-dense material accumulated mainly into membrane delimited vacuoles or lysosomes (Fig. 7C), forming dense areas of high electron contrast (arrows). The EDX microanalysis of this selected area revealed that the overall amount of Cu was 10.88 ± 0.14% weight (or 2.51 ± 0.14% atoms), the complementary counts corresponded to C, O, N, and S. STEM imaging of Cu/Htma treated cell after 5 h revealed signs of apoptotic responses, including blebbing and chromatin condensation (Fig. 7E and F).

Htma causes copper hyperaccumulation to lysosomes

We investigated the accumulation of Cu into vacuoles or lysosomes using fluorescent probes. A commercially available transduction agent (CellLight® Lysosomes-GFP, BacMam 2.0) was chosen to tag lysosomes for confocal microscopy. This transduction method expresses LAMP1 (lysosomal associated membrane protein 1) fused to GFP. Copper Fluor-4 (CF4) and Control Copper Fluor-4 Sulfur 2 (CTRL-CF4-S2) probes were used to detect labile Cu (I).[58] CF4 is a fluorescent dye with a strong response as well as high selectivity for Cu(I) with a long history of optimization.[59]

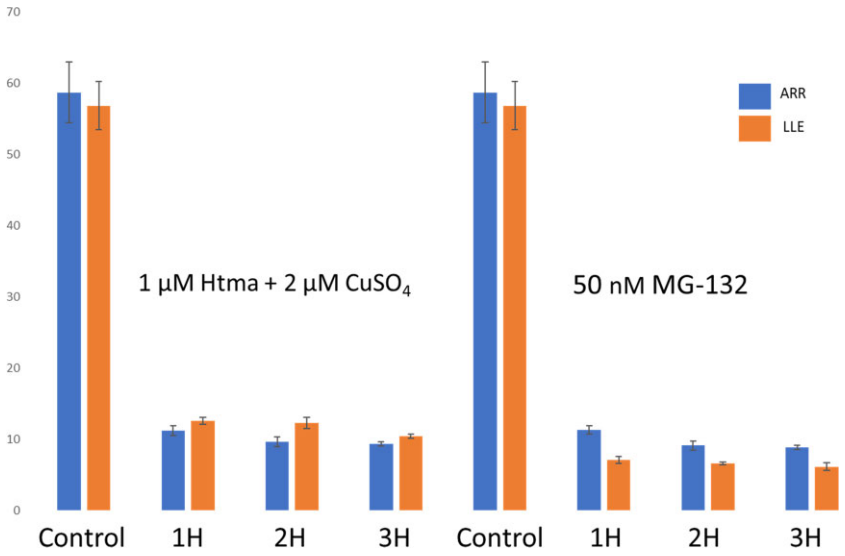

Fig 10 Time course analysis of proteasomal activity in presence of both $Cu(tma)_2$ complex and proteasome inhibitor MG132 in cell lysate of A375 melanoma cells in metal-chelated media.

As Fig. 8 indicates, after 2 h of Cu/Htma treatment, a strong signal for Cu(I) co-localizes with the LAMP1-GFP signal, with reduced signals seen in the control and copper-only treatments. This fluorescent data indicate that the superstoichiometric Cu is reduced to Cu(I) and accumulated within lysosomes.

Ionophore localization

A fluorescent analog, the Zn complex of dithiomaltol, $Zn(ttma)_2$,[37] was used to determine where the metal-complexed ionophore accumulates within the treated cells. In unchelated media complex, $Zn(ttma)_2$ shows strong apoptotic response to A375 and minimal toxicity to normal melanocytes at submicromolar concentrations, and the strong fluorescence allows its uptake to followed by flow cytometry of treated cells (Supplemental Fig. S5). Confocal imaging of $Zn(ttma)_2$ treated A375 cells shows that the fluorophore appears localized in cell membranes and within large vacuoles or lysosomes (Fig. 9).

Cu/Htma treatment inhibits proteasomal activity concurrent with cell death

To determine to what extent Cu/Htma treatment could act as an inhibitor of the proteasome, we assayed proteasomal activity by following the fluorescent quenching of two fluorogenic proteasome substrates: Z-ARR-AMC (Z-Ala-Arg-Arg-amido-4-Methylcoumarin) to test for trypsin-like activity and Z-LLE-AMC (Z-Leu-Leu-Glu-7-amido-4-methylcoumarin) to test for caspase-like post-glutamate peptide hydrolase of the 26S proteasome or 20S proteolytic core. A375 cell lysate was drugged with 0.5% DMSO, 1 μM Htma + 2 μM $CuSO_4$, or 50 nM MG-132 for 1-, 2-, or 3-h increments. Figure 10 shows Cu/Htma is a strong inhibitor of proteasomal activity similar to MG132 with fluorescent quenching after 1 h.

A second set of experiments compared the ubiquitination and viability status of intracellular proteins after treatment with MG132 and Cu/Htma after 2 and 4 h using Western Blotting and MTT staining under the same conditions. As Fig. 11 shows, 2 and 4 h after either MG132 or Cu/Htma treatment display significant increases in ubiquitinated proteins, copper as a treatment alone causes no cell death or appreciable ubiquitination among cellular proteins (supplemental Fig. S6).

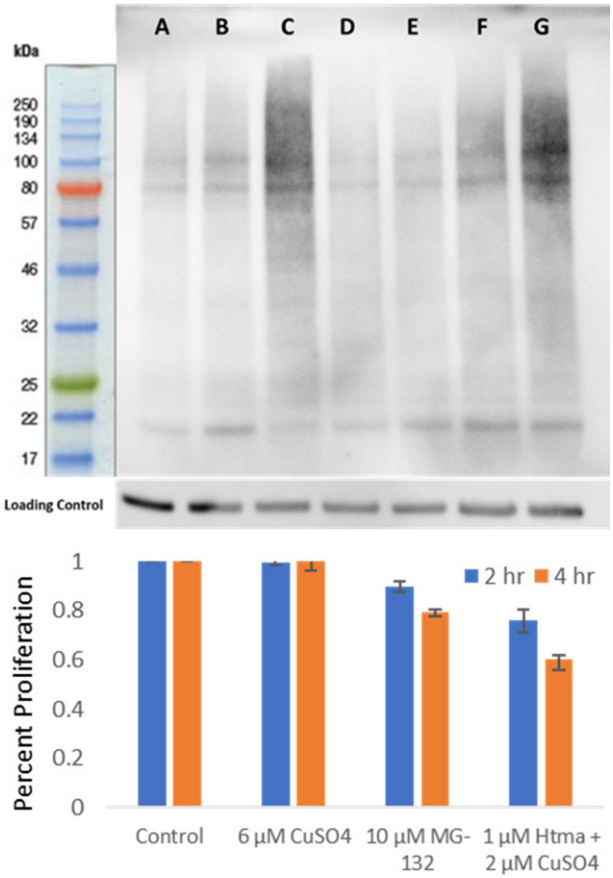

Fig. 11 Effects of Cu/Htma treatment and MG132 on ubiquitinated and cell viability in A375 melanoma. (Top) cells were treated with vehicle 0.5% DMSO (A) and 10 μM MG132 for 2 h (B) or 4 h (C), 2 μM $CuSO_4$ for 2 h (D) or 4 h (E), 1 μM Htma + 2 μM $CuSO_4$ for 2 h (F) or 4 h (G). (Bottom) measurement of cell viability by MTT assay under equivalent conditions. More data are presented in **S6**.

Discussion

Although many Cu chelates show toxicity towards specific cancer cell lines, the Cu/Htma toxicity to melanoma is unusual in that

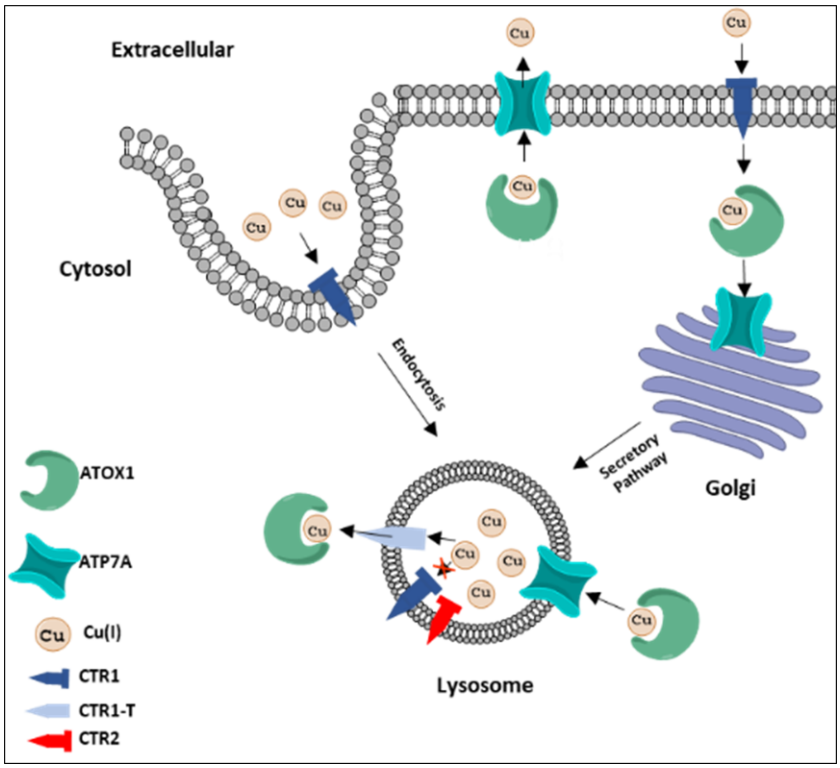

Scheme 2 Intracellular copper trafficking tied to lysosome formation.

the onset of apoptosis is quite rapid and correlates with both the accumulation of intracellular Cu(I) in lysosomes as well as inhibition of the proteosome. The speed of these effects argues against ligand cycling, i.e. extracellular $Cu(tma)_2$ formation and uptake into the cell, followed reduction to Cu(I) and extrusion of Htma. The presence of Cu/Htma engenders the rapid accumulation of Cu, on the timescale of lysosomal formation,[60] but in large excess to the ionophore. Likewise, the increased ubiquitination with increasing Cu concentrations, but independent of stoichiometric Htma, argues against a discrete Cu/Htma complex as the source of proteasomal inhibition.

Lysosomes have a significant role in Cu homeostasis, aiding in both sequestration and compartmentalization of the biometal (Scheme 2).[61] The uptake of Cu proceeds through endocytosis, utilizing lysosomes as vessels for abstracting needed metal ions. In mammals, all membrane-bound Cu transporters such as CTR1, ATP7A/ATP7B, and CTR2 are within the lysosomal membrane to aid Cu influx and efflux. ATP7A/ATP7B are trafficked to the lysosome from the Golgi through the secretory pathway, to pump Cu from cytosolic Cu-binding chaperones like ATOX1 or glutathione into the lysosome. CTR1, in a complementary role, is endocytotically trafficked to the lysosomal membrane to efflux Cu from the lysosome to the cytosolic Cu-chaperones. CTR2, a CTR1 homologue, exerts regulatory control over CTR1 in the lysosomal membranes.[62] Thus, the rapid accumulation of Cu in lysosomes after Cu/Htma treatment may be due to a disruption of one of these critical Cu trafficking pathways.

Other reports of Cu accumulation in lysosomes or small organelles are associated with disruption of metal homeostasis.[63] Zn starvation in *Chlamydomonas*, a common model eukaryote for studies of metal homeostasis, causes Cu accumulation in specialized foci that act as chemical traps for the metal, described as Cu starvation due to compartmentalization.[63] Additionally, inhibition of lysosomal SLC46A3, a solute carrier with unknown function or substrate, caused cytosolic copper deficiency and subsequent mitochondrial dysfunction resulting in both lower lipid catabolism and hepatic lipid accumulation.[64] In another report, $CTR2^{-/-}$ mice exhibit Cu accumulation in intracellular foci that are much smaller in size than in Htma-treated melanoma, but importantly this accumulation does not lead to apoptosis or cell death.[62]

Conclusions

The ionophore Htma shows rapid and Cu-dependent toxicity against A375 melanoma, generating an apoptotic response at submicromolar concentrations. Like other Cu ionophores with anticancer activity, the Cu/Htma treatment shows inhibition of the proteasome comparable to that of the known inhibitor MG132, and which correlates with the onset of apoptosis. This proteasomal inhibition increases with excess Cu, independent of the Htma concentration. Subcellular imaging by electron microscopy (EM) shows that apoptosis is concurrent with rapid Cu accumulation in lysosomes. Imaging of cells treated with the fluorescent analog $Zn(ttma)_2$ shows its accumulation within cellular membranes and lysosomes. The localization suggests the Cu transport system within the lysosome may be a source of ER stress associated with the rapid proteasomal inhibition and apoptotic response.

Experimental

Materials

Chemicals and solvents were obtained from Sigma-Aldrich and Fisher Scientific and were used as received. All solvents were reagent grade. The ionophore Htma and its complexes $Cu(tma)_2$, $Ni(tma)_2$, $Zn(tma)_2$, and $Fe(tma)_3$ were synthesized followed procedures in references.[39,40] The ionophore Httma and its complex $Zn(ttma)_2$ were generated as described in references.[41,43] All

complexes were recrystallized from MeOH, and stock solutions were dissolved in DMSO and frozen until use.

Cells and media

A375 (ATCC® CRL-1619™) cells were purchased from ATCC and cultured in Dullbecco's Modified Eagle's Medium (DMEM) GlutaMAX™ with 10% (FBS), 100 I.U./ml penicillin/100 (μg/ml) streptomycin, and 8 μg/ml gentamicin. Cells were passaged using StemPro™ Accutase™ Cell Dissociation Reagent (ThermoFisher) at approximately 80% confluency to ensure log phase growth.

Melanocytes were processed from pooled neonatal foreskins and cultured in MCDB 153 (Sigma, St Louis, MO) medium containing 2% fetal calf serum, 0.15% bovine pituitary extract (Clonetics, San Diego, CA), 10 ng/ml phorbol myristate-13-acetate, 2 mM calcium chloride, 10 μg/ml insulin, 150 U/ml penicillin, 0.15 mg/ml streptomycin, and 0.1 mM 3-isobutylmethylzanthine (Sigma-Aldrich, St Louis, MO).

The chelated medium used for certain experiments contained fetal calf serum that had been treated with Chelex 100 (Sigma-Aldrich, St Louis, MO) for 1 h at 4°C. The chelated medium substituted fetal calf serum for all newborn calf serum as well, while all the other components remained the same.

Drugs were dissolved in the culture medium or in dimethyl sulfoxide (DMSO) and added to the culture directly. Control samples were added with the same amount of medium and DMSO equivalent to that in the drugged samples. The DMSO in the cell media was <0.5%.

Briefly, cells were trypsinized, washed twice in PBS, and resuspended in binding buffer at a concentration of 1×10^6 cells/ml, of which 100 μl was incubated with 5 μl of Annexin V (AV) conjugated to FITC (Molecular Probes, Eugene, OR) and 75 μM (10 μl) propidium iodide (PI) for 15 min at room temperature in the dark. Cells were then analyzed by flow cytometry using a Becton-Dickinson FACScan. The proportion of apoptotic cells was estimated by the percentage of cells that stained positive for AV while remaining impermeable to PI (AV+/PI–), necrosis was defined as a positive stain with both AV and PI (AV+/PI+), and viability was defined as AV–/PI–. Trypan blue stain was also used in parallel, and the percentage of trypan blue positive cells was similar to the sum of the percentages of AV+/PI– and AV+/PI+ cells. This method was based on the previously published literature where, in the early stages of apoptosis, phosphatidylserine (PS) is translocated from the inner to the outer leaflet of the plasma membrane at the cell surface. Annexin V has a high affinity for PS binding on the cell surface. In late stage of cell death, membrane integrity is lost and propidium iodide can be taken up.

Flow cytometry

Cells were treated with $M(tma)_2$ or Cu/Htma mixtures dissolved in DMSO or water for 24 h. Following trypsinization, cells were washed with cold phosphate-buffered saline (PBS), and centrifuged at 300 × g. Cells were then resuspended in annexin-binding buffer (10 mM HEPES, 140 mM NaCl, and 2.5 mM $CaCl_2$, pH 7.4), and prepared using a Dead Cell Apoptosis Kit with Annexin V FITC and PI, for flow cytometry kit (BD Biosciences). Cell density was diluted to 1×10^6 cells/ml, 5 μl of the annexin V conjugate and 1 μl of 100 μg/ml PI was added to 100 μl of cell solution, and cells were incubated at room temperature for 15 min. After the incubation period, 400 μl of annexin-binding buffer was added to the samples and stored on ice until analysis. A total of 10 000 events were analyzed via flow cytometry using a BD Biosciences FACSVerse system equipped with 488 nm and 640 nm lasers.

MTT assays. The effect of divalent $M(tma)_2$ complexes on a panel of cell lines including A375 WM3211 SK-Mel5 SK- Mel28 and NHDF was assessed using the MTT assay. Cells were seeded at an approximate concentration of 5×10^4 cells/well in a 96-well plate. Appropriate concentrations of $M(tma)_2$ were added and compared to a 0.1% DMSO vehicle control. Cells were placed in a cell culture incubator for 24 h at 37°C and 5% CO_2. After the incubation period, 10 μl of the MTT labeling reagent (final concentration 0.5 mg/ml) was added to each well and incubated for 4 h in the previously mentioned cell culture incubator. An amount of 100 μl of the solubilization solution was then added into each well (for a total of 200 μl), and experiments were allowed stand overnight in the incubator in a humidified atmosphere (e.g. +37°C, 5–6.5% CO_2). After complete solubilization of the formazan crystals, samples were measured and recorded for absorbance at 560 nm to determine cell viability. The IC_{50} were determined using GraphPad Prism 6, fitted into 'Sigmoidal, 4PL, X is log(M)' model.

ICP-MS Cu quantification

A375 cells were drugged in triplicate with $CuSO_4$ and Htma for 24 h in Nunc 12-well plates, trypsinized, washed with PBS, and resuspended in 100 μl RIPA Lysis and Extraction Buffer (Thermo Fisher) with cOmplete™ Protease Inhibitor Cocktail (Sigma-Aldrich) in 50 ml Digestion Vessels (Environmental Express). A sample of each sample was removed and aliquoted for protein quantification using a Pierce™ BCA Protein Assay Kit. The remaining 90 μl of cell suspension was mixed with 90 μl of trace metal grade nitric acid (Fisher Chemical) and digested overnight. The mixture was then heated for 30 min at 80°C, cooled to room temperature, and diluted with 1820 μl of nanopure laboratory grade water. A lysis buffer sample was prepared in the same manner as a method control. ^{63}CU and ^{65}Cu isotopes were measured using an Agilent ICP-MS 790063Cu. An ICP-MS Internal standard mix (Bi, ge, In, Li^6, Lu, Rh, Sc, Tb; Agilent Technologies) was diluted to 100 ppb to identify any instrumental drift or matrix effects. A Copper AA standard (Agilent Technologies) was used to prepare a calibration curve from 1 to 100 ppb.

Preparation of cells for EM

To prepare cells for EM, A375 cells were grown in 10% DMEM chelated media, and supplemented with 2.5 uM $CuCl_2$. Cells were then treated with 0.8 uM Htma or an equivalent amount of DMSO. At hourly intervals over 6 h, cells were treated with accutase, and then fixed by resuspension in 1 ml of 4% paraformaldehyde (Electron Microscopy Sciences) for 15 min before being centrifuged at 1000 g for 5 min. Samples were frozen at –80°C until harvested for examination.

EM and microanalysis

A375 cells dosed with Htma were collected by centrifugation (800 rpm) for 5 min and fixed (PBS buffer with 4% formaldehyde and 1% glutaraldehyde) for 1 h at room temperature, and then stored at 4°C. For SEM imaging, samples were rinsed twice with PBS for 15 min, then post-fixed with 0.5% OsO_4 (Electron Microscopy Sciences) in PBS for 1 h, dehydrated with ethanol series (10, 50, 75, 95, and 100%, 15 min each), and then mounted on ultraflat silicon wafer 5 × 5 mm chips (Ted-Pella). Cells were dried with liquid carbon dioxide for 16 cycles at low speed with an automated Critical Point Dryer (Leica EM CPD300) and stored in a desiccator until imaging. For STEM and EDX microanalysis, the fixed samples were centrifuged at 800 rpm for 10 min to form a pellet. The pellets were rinsed twice with PBS for 15 min,

post-fixed with 0.5% OsO_4 (Electron Microscopy Sciences) in PBS for 1 h, and then dehydrated with ethanol series (10, 50, 75, 95, and 100%, 15 min each). Pellets were washed twice in propylene oxide to remove ethanol, then infiltrated with 50% LX112 resin: propylene oxide (Ladd Research) for 1 h, and finally, the samples were infiltrated with 100% LX112 resin and cured for 48 h at 60°C. Ultrathin sections of 95 nm were obtained with an Ultracut Leica ultramicrotome using a 45° diamond knife (Diatome). The ultrathin sections were mounted on 300 mesh regular nickel grids (Electron Microscopy Sciences), dried on a hotplate at 37°C, and stored in a desiccator until imaging. SEM, STEM, and EDX microanalysis were performed with a S = 5500 in-lend UHR-FE-SEM (Hitachi High Technologies) coupled with a Duo BF/DF-STEM detector, and a solid-state EDX detector (Bruker) operated with an accelerated voltage of 5-10 kV for SEM and 30 kV for STEM/EDX. Micrographs were recorded and analyzed with Quarts PCI, and X-ray microanalysis were acquired and analyzed with QUANTAX (Bruker).

Fixed cell imaging of intracellular Cu

Cells were imaged using an Olympus Confocal Laser Scanning Biological Microscope FV-1000 and processed with Fluoview (FV10-ASW4.1). Cover slips were coated with poly-l-lysine and seeded with A375 cells in 24-well plates before being transduced with LAMP1-GFP (CellLight® Lysosomes-GFP, BacMam 2.0; ThermoFisher) for 48 h. Wells were then treated with Cu/Htma for 2 h followed by incubation for 10 min at 37°C with 2 μM CF4 and 2 μM CTRL-CF4-S2 Cu probes. Cover slips were then washed with PBS and washed three times with cold PBS and fixed with a 4% formaldehyde solution for 20 min at room temperature before being mounted with DAPI on microscope slides (ProLong™ Gold Antifade Mountant with DAPI; ThermoFisher). DAPI signal was visualized using a UV-diode laser at 405 nm, LAMP-1 using the Ar laser at 488 nm, and CF4-Cu(I)/CTRL-CF4-S2 using the He laser at 543 nm.

Proteasomal activity assay

A375 cells were grown in 6-well plates to 70–80% confluency and subsequently drugged with 0.5% DMSO, 1 μM Htma + 2 μM $CuSO_4$, or 50 nM MG-132 for 1-, 2-, or 3-h increments. Cell were then trypsinized and resuspended in 400 μl lysis buffer with 5 mM DTT in centrifuge tubes before being centrifuged at 16,000 × g for 10 min at 4°C. A total of 10 mM stock concentrations of Z-ARR-AMC and Z-LLE-AMC were prepared in DMSO. Cell lysates were measured for protein using a BCA assay; 25 μg of protein of these samples were added to assay buffer [50 mM HEPES (pH 7.8), 10 mM NaCl, 1.5 mM $MgCl_2$, 1 mM EDTA, 250 mM sucrose, 5 mM DTT] to a total volume of 50 μl in centrifuge tubes. These cell fractions were then added to black-walled, clear-bottom 96-well plates followed by 10 μl of 240 μM proteasome substrates to yield a final concentration of 40 μM substrates. After 1-h incubation at 37°C, Z-LLE-AMC treated cells were measured (ex. 350 nm, em. 450 nm) and Z-ARR-AMC treated cells were measured (ex. 370 nm, em. 445 nm.) using a Thermo Varioskan LUX Multimode Microplate Reader to record peak fluorescent intensity.

Analyses of ubiquitinated proteins

Cells were treated with Cu/HtmaCl_2 mixtures or MG132 (Cell Signalling) for 2 and 4 h before the cells were harvested with Accutase™ (Thermo Fisher). Cell lysates were prepared under denaturing conditions to maintain the ubiquitination status of proteins. Cell pellets were in RIPA™ Lysis and Extraction Buffer (Thermo Fisher) supplemented with protease inhibitor cocktail cOmplete™. Protein concentration of lysates was determined by BCA™ assay and subsequently equal amounts of protein were separated using NuPAGE™ 4–12% Bis-Tris Gels and transferred to Amersham Hybond™ PVDF membranes, Ubiquitinated proteins were detected using rabbit-anti-ubiquitin primary antibody (Cell Signaling), anti-rabbit Alexa-Fluor 488 secondary antibody (Cell Signaling), and Amersham ECL™ Prime Western Blotting Detection Reagent.

Supplementary material

Supplementary data are available at *Metallomics* online.

Acknowledgements

We greatly appreciate the assistance and support provided by the Baylor University Center for Microscopy and Imaging and Molecular Biosciences Center, as well as Dr Jefferson Chan.

Funding

P.J.F. acknowledges financial support of Penrose TherapeuTx, and C.J.C. acknowledges funding from NIH GM 79465.

Conflicts of interest

There are no conflicts of interest to declare.

Data availability

Data available on request.

References

1. G. P. Guy, Jr, S. R. Machlin, D. U. Ekwueme and K. R. Yabroff, Prevalence and costs of skin cancer treatment in the U.S., 2002– 2006 and 2007– 2011, *Am. J. Prev. Med.*, 2015, 48 (2), 183–187.
2. G. P. Guy, Jr, C. C. Thomas, T. Thompson, M. Watson, G. M. Massetti and L. C. Richardson, Vital signs: melanoma incidence and mortality trends and projections—United States, 1982–2030, *MMWR Morb. Mortal. Wkly. Rep.*, 2015, 64 (21), 591–596.
3. K. G. Paulson, D. G. Teresa, S. Kim, J. R. Veatch, D. R. Byrd, S. Bhatia, K. Wojcik, A. G. Chapuis, J. A. Thompson, M. M. Madeleine and J. M. Gardner, Age-specific incidence of melanoma in the United States, *JAMA Dermatol.*, 2020, 156 (1), 57–64.
4. H. Davies, G. R. Bignell, C. Cox, P. Stephens, S. Edkins, S. Clegg, J. Teague, H. Woffendin, M. J. Garnett, W. Bottomley, N. Davis, E. Dicks, R. Ewing, Y. Floyd, K. Gray, S. Hall, R. Hawes, J. Hughes, V. Kosmidou, A. Menzies, C. Mould, A. Parker, C. Stevens, S. Watt, S. Hooper, R. Wilson, H. Jayatilake, B. A. Gusterson, C. Cooper, J. Shipley, D. Hargrave, K. Pritchard-Jones, N. Maitland, G. Chenevix-Trench, G. J. Riggins, D. D. Bigner, G. Palmieri, A. Cossu, A. Flanagan, A. Nicholson, J. W. C. Ho, S. Y. Leung, S. T. Yuen, B. L. Weber17, H. F. Seigler, T. L. D, H. Paterson, R. Marais, C. J. Marshall, R. Wooster, M. R. Stratton and P. A. Futreal, Mutations of the BRAF gene in human cancer, *Nature*, 2002, 417, (6892), 949–954.
5. D. C. Brady, M. S. Crowe, M. L. Turski, G. A. Hobbs, X. Yao, A. Chaikuad, S. Knapp, K. Xiao, S. L. Campbell, D. J. Thiele and C. M. Counter, Copper is required for oncogenic BRAF signalling and tumorigenesis, *Nature*, 2014, 509 (7501), 492–496.
6. M. L. Turski, D. C. Brady, H. J. Kim, B.-E. Kim, Y. Nose, C. M. Counter, D. R. Winge and D. J. Thiele, A novel role for copper

in Ras/mitogen-activated protein kinase signaling, *Mol. Cell. Biol.*, 2012, 32 (7), 1284–1295.
7. M. C. Linder, *Biochemistry of Copper*, Springer Science & Business Media, 2013, Vol. 10.
8. J. L. Allensworth, M. K. Evans, F. Bertucci, A. J. Aldrich, R. A. Festa, P. Finetti, N. T. Ueno, R. Safi, D. P. McDonnell, D. J. Thiele, S. V. Laere and G. R. Devi, Disulfiram (DSF) acts as a copper ionophore to induce copper-dependent oxidative stress and mediate anti-tumor efficacy in inflammatory breast cancer, *Mol. Oncol.*, 2015, 9 (6), 1155–1168.
9. X. Chen, X. Zhang, J. Chen, Q. Yang, L. Yang, D. Xu, P. Zhang, X. Wang and J. Liu, Hinokitiol copper complex inhibits proteasomal deubiquitination and induces paraptosis-like cell death in human cancer cells, *Eur. J. Pharmacol.*, 2017, 815 (15), 147–155.
10. D. Cen, R. I. Gonzalez, J. A. Buckmeier, R. S. Kahlon, N. B. Tohidian and F. L. Meyskens, Jr, Disulfiram induces apoptosis in human melanoma cells: a redox-related process, *Mol. Cancer Ther.*, 2002, 1 (3), 197–204.
11. J. R. Kirshner, S. He, V. Balasubramanyam, J. Kepros, C.-Y. Yang, M. Zhang, Z. Du, J. Barsoum and J. Bertin, Elesclomol induces cancer cell apoptosis through oxidative stress, *Mol. Cancer Ther.*, 2008, 7 (8), 2319–2327.
12. D. Cen, D. Brayton, B. Shahandeh, F. L. Meyskens and P. J. Farmer, Disulfiram facilitates intracellular Cu uptake and induces apoptosis in human melanoma cells, *J. Med. Chem.*, 2004, 47 (27), 6914–6920.
13. P. J. Farmer, S. Gidanian, B. Shahandeh, A. J. D. Bilio, N. Tohidian and F. L. Meyskens, Jr, Melanin as a target for melanoma chemotherapy: pro-oxidant effect of oxygen and metals on melanoma viability, *Pigm. Cell Res.*, 2003, 16 (3), 273–279.
14. Y.-W. Chen, K.-L. Chen, C.-H. Chen, H.-C. Wu, C.-C. Su, C.-C. Wu, T.-D. Way, D.-Z. Hung, C.-C. Yen, Y.-T. Yang and T.-H. Lu, Pyrrolidine dithiocarbamate (PDTC)/Cu complex induces lung epithelial cell apoptosis through mitochondria and ER-stress pathways, *Toxicol. Lett.*, 2010, 199 (3), 333–340.
15. K. G. Daniel, P. Gupta, R. H. Harbach, W. C. Guida and Q. P. Dou, Organic copper complexes as a new class of proteasome inhibitors and apoptosis inducers in human cancer cells, *Biochem. Pharmacol.*, 2004, 67 (6), 1139–1151.
16. N. Liu, C. Liu, X. Li, S. Liao, W. Song, C. Yang, C. Zhao, H. Huang, L. Guan, P. Zhang, S. Liu, X. Hua, X. Chen, P. Zhou, X. Lan, S. Yi, S. Wang, X. Wang, Q. P. Dou and J. Liu, A novel proteasome inhibitor suppresses tumor growth via targeting both 19S proteasome deubiquitinases and 20S proteolytic peptidases, *Sci. Rep.*, 2014, 4 (1), 1–13.
17. K. G. Daniel, D. Chen, S. Orlu, Q. C. Cui, F. R. Miller and Q. P. Dou, Clioquinol and pyrrolidine dithiocarbamate complex with copper to form proteasome inhibitors and apoptosis inducers in human breast cancer cells, *Breast Cancer Res.*, 2005, 7 (6), 1–12.
18. D. B. Lovejoy, P. J. Jansson, U. T. Brunk, J. Wong, P. Ponka and D. R. Richardson, Antitumor activity of metal-chelating compound Dp44mT is mediated by formation of a redox-active copper complex that accumulates in lysosomes, *Cancer Res.*, 2011, 71 (17), 5871–5880.
19. S. Hager, K. Korbula, B. Bielec, M. Grusch, C. Pirker, M. Schosserer, L. Liendl, M. Lang, J. Grillari, K. Nowikovsky, V. F. S. Pape, T. Mohr, G. Szakács, B. K. Keppler, W. Berger, C. R. Kowol and P. Heffeter, The thiosemicarbazone Me2NNMe2 induces paraptosis by disrupting the ER thiol redox homeostasis based on protein disulfide isomerase inhibition, *Cell Death. Dis.*, 2018, 9(11), 1052.
20. A. Southon, K. Szostak, K. M. Acevedo, K. A. Dent, I. Volitaki, A. A. Belaidi, K. J. Barnham, P. J. Crouch, S. Ayton, P. S. Donnelly and A. I. Bush, CuII (atsm) inhibits ferroptosis: implications for treatment of neurodegenerative disease, *Br. J. Pharmacol.*, 2020, 177 (3), 656–667.
21. S. Tardito, I. Bassanett, C. Bignardi, L. Elviri, M. Tegoni, C. Mucchino, O. Bussolati, R. Franchi-Gazzola and L. Marchio`, Copper binding agents acting as copper ionophores lead to caspase inhibition and paraptotic cell death in human cancer cells, *J. Am. Chem. Soc.*, 2011, 133 (16), 6235–6242.
22. Y. Yang, K. Zhang, Y. Wang, M. Li, X. Sun, Z. Liang, L. Wang, L. Chen, H. Yang and L. Zhu, Disulfiram chelated with copper promotes apoptosis in human breast cancer cells by impairing the mitochondria functions, *Scanning*, 2016, 38 (6), 825–836.
23. V. T. Cheriyan, Y. Wang, M. Muthu, S. Jamal, D. Chen, H. Yang, L. A. Polin, A. L. Tarca, H. I. Pass, Q. P. Dou, S. Sharma, A. Wali and A. K. Rishi, Disulfiram suppresses growth of the malignant pleural mesothelioma cells in part by inducing apoptosis, *PLoS One*, 2014, 9 (4), e93711.
24. S. Hassani, P. Ghaffari, B. Chahardouli, K. Alimoghaddam, A. Ghavamzadeh, S. Alizadeh and S. H. Ghaffari, Disulfiram/copper causes ROS levels alteration, cell cycle inhibition, and apoptosis in acute myeloid leukaemia cell lines with modulation in the expression of related genes, *Biomed. Pharmacother.*, 2018, 99, 561–569.
25. B. Xu, S. Wang, R. Li, K. Chen, L. He, M. Deng, V. Kannappan, J. Zha, H. Dong and W. Wang, Disulfiram/copper selectively eradicates AML leukemia stem cells in vitro and in vivo by simultaneous induction of ROS-JNK and inhibition of NF-κB and Nrf2, *Cell Death. Dis.,* 2017, 8 (5), e2797.
26. B. Xu, M. Deng, Z. Jiang, J. Li, K. Chen and P. Li, Role of mitochondrial apoptotic pathway in disulfiram/copper mixture-induced cell apoptosis in human B-lineage acute lymphoblastic leukemia in vitro, *Blood*, 2015, 126 (23), 4920.
27. W. Chen, W. Yang, P. Chen, Y. Huang and F. Li, Disulfiram copper nanoparticles prepared with a stabilized metal ion ligand complex method for treating drug-resistant prostate cancers, *ACS Appl. Mater. Interfaces*, 2018, 10, 41118–41128.
28. R. Gerl and D. L. Vaux, Apoptosis in the development and treatment of cancer, *Carcinogenesis*, 2005, 26 (2), 263–270.
29. S. Elmore, Apoptosis: a review of programmed cell death, *Toxicol. Pathol.*, 2007, 35 (4), 495–516.
30. L. E. Bröker, F. A. Kruyt and G. Giaccone, Cell death independent of caspases: a review, *Clin. Cancer Res.*, 2005, 11 (9), 3155–3162.
31. S. Sperandio, I. D. Belle and D. E. Bredesen, An alternative, non-apoptotic form of programmed cell death, *Proc. Natl. Acad. Sci. USA*, 2000, 97 (26), 14376–14381.
32. Y. Sun, P. Chen, B. Zhai, M. Zhang, Y. Xiang, J. Fang, S. Xu, Y. Gao, X. Chen, X. Sui and G. Li, The emerging role of ferroptosis in inflammation, *Biomed. Pharmacother.*, 2020, 127, 110108.
33. J. S. Roh and D. H. Sohn, Damage-associated molecular patterns in inflammatory diseases, *Immune Netw.*, 2018, 18 (4), e27.
34. Y. Xiao, D. I. Chen, X. Zhang, Q. Cui, Y. Fan, C. Bi and Q. P. Dou, Molecular study on copper-mediated tumor proteasome inhibition and cell death, *Int. J. Oncol.*, 2010, 37 (1), 81–87.
35. A. Chakrabarti, A. W. Chen and J. D. Varner, A review of the mammalian unfolded protein response, *Biotechnol. Bioeng.*, 2011, 108 (12), 2777–2793.
36. A. Fribley, K. Zhang and R. J. Kaufman, Regulation of apoptosis by the unfolded protein response. In: P. Erhardt, A. Toth (eds.), *Apoptosis. Methods in Molecular Biology (Methods and Protocols)*, Vol. 559, Totowa, NJ: Humana Press; 2009.
37. C. Stefani, Z. Al-Eisawi, P. J. Jansson, D. S. Kalinowski and D. R. Richardson, Identification of differential anti-neoplastic activity of copper bis (thiosemicarbazones) that is mediated by intracel-

lular reactive oxygen species generation and lysosomal membrane permeabilization, *J. Inorg. Biochem.*, 2015, 152, 20–37.
38. A. E. Stacy, D. Palanimuthu, P. V. Bernhardt, D. S. Kalinowski, P. J. Jansson and D. R. Richardson, Zinc (II)–thiosemicarbazone complexes are localized to the lysosomal compartment where they transmetallate with copper ions to induce cytotoxicity, *J. Med. Chem.*, 2016, 59 (10), 4965–4984.
39. J. A. Lewis, B. L. Tran, D. T. Puerta, E. M. Rumberger, D. N. Hendrickson and S. M. Cohen, Synthesis, structure and spectroscopy of new thiopyrone and hydroxypyridinethione transition-metal complexes, *Dalton Trans.*, 2005, 15 (15), 2588–2596.
40. J. A. Lewis, D. T. Puerta and S. M. Cohen, Metal complexes of the trans-influencing ligand thiomaltol, *Inorg. Chem.*, 2003, 42 (23), 7455–7459.
41. D. Brayton, F. E. Jacobsen, S. M. Cohen and P. J. Farmer, A novel heterocyclic atom exchange reaction with Lawesson's reagent: a one-pot synthesis of dithiomaltol, *Chem. Commun.*, 2008, 2 (2), 206–208.
42. M. Backlund, J. Ziller and P. J. Farmer, Unexpected C– H activation of Ru (II)– dithiomaltol complexes upon oxidation, *Inorg. Chem.*, 2008, 47 (7), 2864–2870.
43. B. Bruner, M. B. Walker, M. M. Ghimire, D. Zhang, M. Selke, K. K. Klausmeyer, M. A. Omary and P. J. Farmer, Ligand-based photooxidations of dithiomaltolato complexes of Ru (II) and Zn (II): photolytic CH activation and evidence of singlet oxygen generation and quenching, *Dalton Trans.*, 2014, 43 (30), 11548–11556.
44. S. R. Schlesinger, B. Bruner, P. J. Farmer and S.-K. Kim, Kinetic characterization of a slow-binding inhibitor of Bla2: thiomaltol, *J. Enzyme Inhib. Med. Chem.*, 2013, 28 (1), 137–142.
45. D. F. Brayton, Targeting melanoma via metal based drugs: Dithiocarbamates, disulfiram copper specificity, and thiomaltol ligands, Ph.D. Thesis, Irvine: University of California, 2006.
46. Z. Sartor, Synergistic effects of hydroxychloroquine on the activity of thiomaltol against melanoma cancer cells, Ph.D. Thesis, Baylor University, 2012.
47. M. E. Helsel, E. J. White, S. Z. A. Razvi, B. Alies and K. J. Franz, Chemical and functional properties of metal chelators that mobilize copper to elicit fungal killing of Cryptococcus neoformans, *Metallomics*, 2017, 9 (1), 69–81.
48. X. Zhiguang, P. S. Donnelly, M. Zimmermann and A. G. Wedd, Transfer of copper between bis (thiosemicarbazone) ligands and intracellular copper-binding proteins. Insights into mechanisms of copper uptake and hypoxia selectivity, *Inorg. Chem.*, 2008, 47 (10), 4338–4347.
49. N. C. Rath, K. S. Rasaputra, R. Liyanage, G. R. Huff and W. E. Huff, Dithiocarbamate toxicity-an appraisal. In: *Pesticides in the Modern World-Effects of Pesticides Exposure*, 2011, (2011), 323–340.
50. R. Strecker, S. Weigt and T. Braunbeck, Cartilage and bone malformations in the head of zebrafish (Danio rerio) embryos following exposure to disulfiram and acetic acid hydrazide, *Toxicol. Appl. Pharmacol.*, 2013, 268 (2), 221–231.
51. B. A. Mendelsohn, C. Yin, S. L. Johnson, T. P. Wilm, L. Solnica-Krezel and J. D. Gitlin, Atp7a determines a hierarchy of copper metabolism essential for notochord development, *Cell Metab.*, 2006, 4 (2), 155–162.
52. H. Ishizaki, M. Spitzer, J. Wildenhain, C. Anastasaki, Z. Zeng, S. Dolma, M. Shaw, E. Madsen, J. Gitlin, R. Marais, M. Tyers and E. E. Patton, Combined zebrafish-yeast chemical-genetic screens reveal gene–copper-nutrition interactions that modulate melanocyte pigmentation, *Dis. Model Mech.*, 2010, 3 (9-10), 639–651.
53. C. Hagan, Disruption of copper homeostasis by copper chelating agents in embryonic zebrafish, Ph.D. Thesis, Baylor University, 2016.
54. S. Burattini and E. Falcieri, Analysis of cell death by electron microscopy, In: *Necrosis*, Totowa, NJ: Humana Press; 2013, 77–89.
55. S. T. Orta-García, G. Plascencia-Villa, A. C. Ochoa-Martínez, T. Ruiz-Vera, F. J. Pérez-Vázquez, J. J. Velázquez-Salazar, M. J. Yacamán, H. R. Navarro-Contreras and I. N. Pérez-Maldonado, Analysis of cytotoxic effects of silver nanoclusters on human peripheral blood mononuclear cells 'in vitro', *J. Appl. Toxicol.*, 2015, 35 (10), 1189–1199.
56. M. K. White and C. Cinti, A Morphologic Approach to Detect Apoptosis Based on Electron Microscopy, In: A. Giordano, G. Romano (eds.) *Cell Cycle Control and Dysregulation Protocols. Methods in Molecular Biology*™, Vol. 285, Humana Press, 2004.
57. P. Mita, A. D. Luca, L. Abbro and L. Dini, Ultrastructural analysis of apoptosis induced by apoptotic U937 cells conditioned medium, *Ital. J. Zool.*, 2003, 70 (2), 141–146.
58. T. Xiao, C. M. Ackerman, E. C. Carroll, S. Jia, A. Hoagland, J. Chan, B. Thai, C. S. Liu, E. Y. Isacoff and C. J. Chang, Copper regulates rest-activity cycles through the locus coeruleus-norepinephrine system, *Nat. Chem. Biol.*, 2018, 14 (7), 655–663.
59. J. A. Cotruvo, Jr, A. T. Aron, K. M. Ramos-Torres and C. J. Chang, Synthetic fluorescent probes for studying copper in biological systems, *Chem. Soc. Rev.*, 2015, 44 (13), 4400–4414.
60. Y. Han, M. Li, F. Qiu, M. Zhang and Y.-H. Zhang, Cell-permeable organic fluorescent probes for live-cell long-term super-resolution imaging reveal lysosome-mitochondrion interactions, *Nat. Commun.*, 2017, 8 (1), 1–9.
61. E. V. Polishchuk and R. S. Polishchuk, The emerging role of lysosomes in copper homeostasis, *Metallomics*, 2016, 8 (9), 853–862.
62. H. Öhrvik, Y. Nose, L. K. Wood, B.-E. Kim, S.-C. Gleber, M. Ralle and D. J. Thiele, Ctr2 regulates biogenesis of a cleaved form of mammalian Ctr1 metal transporter lacking the copper-and cisplatin-binding ecto-domain, *Proc. Natl. Acad. Sci. USA*, 2013, 110 (46), E4279–E4288.
63. E. J. Ge, A. I. Bush, A. Casini, P. A. Cobine, J. R. Cross, G. M. DeNicola, Q. P. Dou, K. J. Franz, V. M. Gohil, S. Gupta, S. G. Kaler, S, Lutsenko, V Mittal, M. J. Petris, R Polishchuk, M. Ralle, M. L. Schilsky, N. K. Tonks, L. T. Vahdat, L. Van Aelst, D. Xi,, P. Yuan, D. C. Brady and C. J. Chang, Connecting copper and cancer: from transition metal signalling to metalloplasia, *Nat. Rev. Cancer*, 2021, 11, 1–2.
64. A. Hong-Hermesdorf, M. M, S. D. Gallaher, J. Kropat, S. C. Dodani, J. Chan, D. Barupala, D. W. Domaille, D. I. Shirasaki, J. A. Loo, P. K. Weber, J. Pett-Ridge, T. L. Stemmler, C. J. Chang and S. S. Merchant, Subcellular metal imaging identifies dynamic sites of Cu accumulation in Chlamydomonas, *Nat. Chem. Biol.*, 2014, 10 (12), 1034–1042.
65. J.-H. Kim, T. Matsubara, J. Lee, C. Fenollar-Ferrer, K. Han, D. Kim, S. Jia, C. J. Chang, H. Yang, T. Nagano, K. W. Krausz, S.-H. Yim and F. J. Gonzalez, Lysosomal SLC46A3 modulates hepatic cytosolic copper homeostasis, *Nat. Commun.*, 2021, 12 (1), 1–12.